Persistent Homology for Automatic Determination of Human-Data Based Cost of Bipedal Walking

Ram Vasudevan[a], Aaron Ames[b], Ruzena Bajcsy[a]

[a] *Electrical Engineering and Computer Sciences*
University of California at Berkeley
Berkeley, CA 94720
{ramv,bajcsy}@eecs.berkeley.edu
[b] *Mechanical Engineering*
Texas A&M University
College Station, TX 77843
aames@tamu.edu

Abstract

The focus of robotic bipedal walking to date has been the development of anthropomorphic gait, but the community as a whole has struggled to agree on the correct ordering of discrete events during walking. In this paper, we propose a *universal* temporal ordering of discrete events for bipedal walking based on motion capture data collected from a nine subject straight line walking experiment. To construct this ordering, we develop a technique based on persistent homology to process the motion capture data to determine when the number of contact points change during the course of a step which automatically dictates the ordering of discrete events. Surprisingly the findings of this work are that every subject regardless of age, sex, weight or height in the experiment had an *identical* temporal ordering of such events. This result allows for the development of a universal anthropomorphic bipedal robotic walking model because the temporal ordering of events together with the Lagrangian modeling of the robot completely determines the mathematical model of the system. Importantly, this universal ordering allows us to propose a cost function based on human data: the *human-based cost*, which we use to gauge the "human-like" quality of robotic walking.

Keywords: Robotics; Bipedal Robotic Walking; System Identification; Homology

1. Introduction

One of the most important decisions made during the design of a controller for bipedal robots is the temporal ordering of events that occur during the gait, i.e., the discrete phases (or *domains*) of the walking termed a *domain breakdown*. This decision alone determines the constraints that are enforced at any

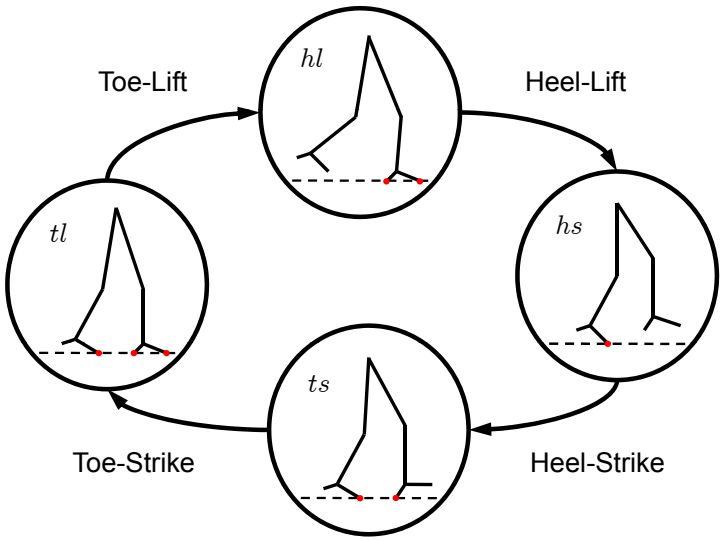

Figure 1: An example of a *domain breakdown*, i.e., the discrete phases of a walking gait based upon a specific temporal ordering. The red dots indicate the constraints enforced in each discrete phase (or domain)

given time during the gait, e.g., the foot being flat on the ground correspondingly determines the continuous dynamics (through holonomic constraints) on each phase and the discrete dynamics (impact equations) between each phase. Therefore, given the equations of motion for a bipedal robot, the temporal ordering of events completely determines the mathematical model for the biped (referred to as *hybrid systems* or *systems with impulsive effects*).

The temporal ordering of events not only determines the underlying mathematical model of a bipedal robot, but it is essential during control design. In each phase of walking the control objectives may be, and often are, dramatically different. For example, for the specific discrete phases given in Fig. 1, it might be desirable to design a control law that transitions from domain $[lh, lt]$ to domain $[lt]$, i.e., a controller that forces the heel to lift. Knowing that such a controller is desirable (or even needed at all) is purely a function of the domain breakdown. In essence, the domain breakdown directly affects the nature of walking.

Currently there exists a fractured landscape in the bipedal walking community when one considers the domain breakdown. Traditionally, most models of bipedal robots have employed a single domain model ([1, 2, 3, 4]), which assumes an instantaneous double support phase and usually excludes the presence of feet (models of this form began with the so-called compass gait biped, which did not have knees or feet). Adding feet to the bipedal robot results in the need to extend the domain breakdown beyond a single discrete phase, which is typically done by either adding a phase where the heel is off the ground or a double

support phase where both feet are on the ground, or any combination thereof [5, 6, 7]. This lack of consistency among models in the literature motivates the desire to determine if there does in fact exist a single "universal" domain breakdown that should be used when modeling bipedal robots, especially in the context of obtaining human-like bipedal walking.

The traditional tact taken to generate human like walking relies upon tracking of motion capture data [8]. Either these methods track a single data point (called the Zero Mass Point) which has been proven insufficient to guarantee even the stability of the generated walking or track the entire data signal which does not allow for the generalization of the generated walking due to different construction, inertial properties, or actuation methods [9]. Human gait has been studied in great depth by the biomechanics community [10, 11, 12]. This work has focused on qualitatively describing the motion and function of various joints during walking [13, 14, 15] or constructed simple linear torsional spring models of specific joints [16]. Unfortunately little has been done to understand how these empirical observations can be employed to construct a mathematical model for gait. Since a robotic and human walker employ such fundamentally different constructs, we begin by describing an appropriate level of abstraction at which to view human walking in order to extract a meaningful mathematical model of robotic gait capable of generating human-like gait. In particular, we begin by showing that the discrete events during walking uniquely determine a dynamical model of gait. The goal of this paper is to then answer the following two questions: (1) *Is there a universal domain breakdown for human-like bipedal walking?* and (2) *Is there a method to quantify how human-like a certain walking gait truly is?*

To address the first question "*Is there a universal domain breakdown for human-like bipedal walking?*" we begin by conducting a nine subject straight line walking motion capture experiment. From this data, we develop a novel and automatic method based on persistent homology for determining the domain breakdown of each subject. The application of homological arguments to hybrid systems is not new [17, 18], but to our knowledge this is the first application of persistent homology to identify a hybrid system model. Importantly, we show that every subject has the same domain breakdown. That is, there is a *universal domain breakdown for human walking*.

To address the second question "*Is there a method to quantify how human-like a certain walking gait truly is?*" this paper proposes a cost function based upon the human-walking data: the *human-based cost*. This cost function is built upon the idea of comparing the *temporal ordering of events* for humans and robots and, more specifically, the amount of time spent in each discrete domain. That is, for a domain breakdown and a walking gait (for either a human or a robot), there is an associated weighted cycle graph, termed a *walking cycle*. We then find the cycle graph and associated weighting that is the minimum distance with respect to a graph metric, the cut distance, between all of the subjects' walking cycles. This *optimal walking cycle* gives a "universal" domain breakdown and associated walking cycle for human walking. Given another walking cycle associated with either a human or a robot, the *human-based cost*

is defined to be the cut distance between this walking cycle and the optimal walking cycle. To demonstrate the utility of the proposed cost function, we compute the human-based cost both for the subjects in the experiment and for existing robotic models. Computing the human-based cost for existing bipedal robotic models confirms that robotic gaits which are more anthropomorphic in nature have a lower human-based cost.

Our contributions are four-fold. First, we show in Section 2 that determining when constraints are enforced also determines the domain breakdown for each subject of the experiment. Second, in Section 3 we develop a motion capture dataset, which we make available, of nine healthy people (exhibiting a wide variety of ages, genders, heights and weights) walking in a straight line. Next, in Section 4, we develop a novel procedure exploiting persistent homology to determine constraint enforcement and hence domain breakdown and show that every subject in our experiment has the *same* domain breakdown illustrated in Fig. 1. Finally, in Sections 5 and 6 we show that by constructing an appropriate metric over the space of domain breakdowns that we can construct a cost function that when minimized produces anthropomorphic gait.

2. From Constraints to Models

Bipedal robots display both discrete and continuous behavior, i.e., they are naturally modeled as *hybrid systems*. Bipeds evolve in a continuous fashion according to traditional equations of motion when a fixed number of points on the biped are in contact with the ground, e.g., when one foot is flat on the ground while the other swings forward. The discrete behavior in the system occurs when the number of contact points changes.

In this section, we formally introduce hybrid systems and discuss how the equations of motion of a robot together with a temporal ordering of constraints completely determines the hybrid model of the system. That is, when modeling bipedal robots, one needs only the Lagrangian of the robot and a domain breakdown.

2.1. Hybrid Systems.

Hybrid systems (or *systems with impulse effects*) have been studied extensively in a wide variety of contexts and have been utilized to model a wide range of bipedal robotic models. In this section, we introduce a definition of a hybrid system applicable to bipedal walking.

Graphs and Cycles. A graph is a tuple $\Gamma = (V, E)$, where V is the set of vertices and $E \subset V \times V$ is the set of edges; an edge $e \in E$ can be written as $e = (i, j)$, and the source of e is $\text{source}(e) = i$ and the target of e is $\text{target}(e) = j$. Since steady state bipedal walking naturally appears periodic, we are interested in hybrid systems *on a cycle*; therefore, we are interested in graphs that contain cycles or are themselves cycles. A *directed cycle* (or just a cycle) is a graph

$\ell = (V, E)$ such that the edges and vertices can be written as:

$$\begin{aligned} V &= \{v_0, v_1, \ldots, v_{p-1}\}, \\ E &= \{e_0 = (v_0, v_1), \ldots, e_{p-1} = (v_{p-1}, v_0)\}. \end{aligned} \tag{1}$$

Since in the case of a cycle, the edges are completely determined by the vertices, we sometimes simply denote a cycle by:

$$\ell : \ v_0 \to v_1 \to \cdots \to v_{p-1}$$

In the case when a graph Γ is being considered with more than one cycle, we denote a cycle in the graph by $\ell \subset \Gamma$.

Example 1. *The domain graph pictured in Fig. 1 has an underlying graph that is a directed cycle: $\Gamma_u = (V_u, E_u)$. In particular, there are 4 vertices and edges, which results in the cycle:*

$$\ell_u : \ [lh, lt] \to [lt] \to [lt, rh] \to [lt, rh, rt].$$

With the notion of a directed cycle, we can introduce the formulation of a hybrid system that is of interest in this paper.

Definition 1. *A* hybrid system in a cycle *is a tuple*

$$\mathscr{HC} = (\ell, D, U, S, \Delta, FG),$$

where

- *$\ell = (V, E)$ is a directed cycle*
- *$D = \{D_v\}_{v \in V}$ is a set of domains, where $D_v \subseteq \mathbb{R}^{n_v} \times \mathbb{R}^{m_v}$ is a smooth submanifold of $\mathbb{R}^{n_v} \times \mathbb{R}^{m_v}$ (with $\mathbb{R}^{m_v}$ representing control inputs),*
- *$U = \{U_v\}_{v \in V}$, where $U_v \subset \mathbb{R}^{m_v}$ is a set of admissible controls,*
- *$S = \{S_e\}_{e \in E}$ is a set of guards, where $S_e \subseteq D_{\text{source}(e)}$,*
- *$\Delta = \{\Delta_e\}_{e \in E}$ is a set of reset maps, where $\Delta_e : \mathbb{R}^{n_{\text{source}(e)}} \to \mathbb{R}^{n_{\text{target}(e)}}$ is a smooth map,*
- *$FG = \{(f_v, g_v)\}_{v \in E}$, where (f_v, g_v) is a control system on D_v, i.e., $\dot{x} = f_v(x) + g_v(x)u$ for $x \in D_v$ and $u \in U_v$.*

2.2. Hybrid Systems from Constraints.

The remainder of this section discusses how a Lagrangian for the biped together with domain breakdown (which determines the active constraints on each vertex of a directed cycle) allows one to explicitly construct a hybrid model of the system. Many details of this construction are extensions of results presented in [19].

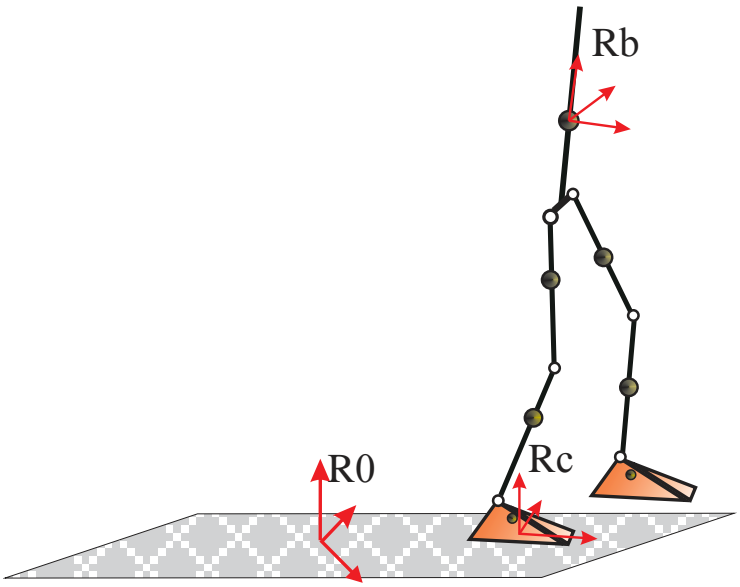

Figure 2: An illustration of the placement of coordinate systems used during the derivation of the Lagrangian.

2.2.1. General Setup

We begin with a bipedal robot in three dimensions—the discussion in this paper is applicable to the two dimensional case. We first construct a Lagrangian for the biped when no assumptions on ground contact are made and then enforce the ground contact conditions through constraints.

Lagrangians. As in Fig. 2, let R_0 be a fixed inertial or world frame, and R_b be a reference frame attached to the body of the biped with position $p_b \in \mathbb{R}^3$ and orientation $\phi_b \in SO(3)$. Consider a configuration space for the biped Q_r, i.e., a choice of (body or shape) coordinates for the robot where typically $q_r \in Q_r$ is a collection of (relative) angles between each successive link of the robot. The evolution of the *generalized* coordinates of the robot are then given by $q : [0, \infty) \to Q = \mathbb{R}^3 \times SO(3) \times Q_r$, with Q the generalized configuration space.

The Lagrangian of a bipedal robot, $L : TQ \to \mathbb{R}$, can be stated in terms of kinetic and potential energies as:

$$L(q(t), \dot{q}(t)) = K(q(t), \dot{q}(t)) - V(q(t)), \tag{2}$$

where $(q(t), \dot{q}(t)) \in TQ$. The Euler-Lagrange equations yield the equations of motion, which for robotic systems are stated as:

$$D(q(t))\ddot{q}(t) + H(q(t), \dot{q}(t)) = B(q(t))u(t), \tag{3}$$

where $D(q(t))$ is the inertia matrix, $B(q(t))$ is the torque distribution matrix, $B(q(t))u(t)$ is the vector of actuator torques and $H(q(t), \dot{q}(t))$ contains the Coriolis, gravity terms and non-conservative forces grouped into a single vector [20].

Contact Points. The continuous dynamics of the system depend on which constraints are enforced at any given time, while the discrete dynamics depend on the change in constraints. Constraints and their enforcement are dictated by the number of contact points of the system with the ground or itself. Specifically, we define the *set of contact points* as set $\mathcal{C} = \{c_1, c_2, \ldots, c_k\}$, where each c_i is a specific type of contact possible in the biped, either with the ground or in the biped itself (such as the knee locking). Ignoring the knees there are four contact points of interest given by:

$$\mathcal{C} = \{lh, lt, rh, rt\}$$

where lh and lt indicate the left heel and toe, and rh and rt indicate right heel and toe, respectively.

Constraints. Contact points introduce a *holonomic constraint* on the system, η_c for $c \in \mathcal{C}$, which is a vector valued function $\eta_c : Q \to \mathbb{R}^{n_c}$, that must be held constant for the contact point to be maintained, i.e., $\eta_c(q(t)) = \text{constant} \in \mathbb{R}^{n_c}$ fixes the contact point but allows rotation about this point if feasible. It is useful to express the collection of all holonomic constraints in a single matrix $\eta(q(t)) \in \mathbb{R}^{n \times |\mathcal{C}|}$ as:

$$\eta(q(t)) = \begin{bmatrix} \eta_{lh}(q(t)) & 0 & 0 & 0 \\ 0 & \eta_{lt}(q(t)) & 0 & 0 \\ 0 & 0 & \eta_{rh}(q(t)) & 0 \\ 0 & 0 & 0 & \eta_{rt}(q(t)) \end{bmatrix}$$

where $n = \sum_{c \in \mathcal{C}} n_c$.

In the case of foot contact, consider a reference frame R_c at the contact point $c \in \{lh, lt, rh, rt\}$ such that the axis of rotation about this point (either the heel or toe) is in the z direction (the axis pointing up) as illustrated in Fig. 2. Then the rotation matrix between R_0 and R_c can be written as the product of three rotation matrices $Rot(x, \phi_c^z)Rot(y, \phi_c^y)Rot(z, \phi_c^z)$ and the position and orientation of R_c relative to R_0 is given as

$$\eta_c(q) = \begin{bmatrix} p_c(q(t)) \\ \phi_c^x \\ \phi_c^y \end{bmatrix}$$

where the first argument to *Rot* denotes the axis of orientation and the second argument to *Rot* denotes the amount of rotation and $p_c(q(t))$ is the position of c. Since ϕ_c^z is free to move while ϕ_c^x and ϕ_c^y must be held constant, the end result of this choice of coordinates is a holonomic constraint $\eta_c(q(t)) = \text{constant}$, which fixes the foot contact point to the ground but allows rotation about the heel or toe depending on the specific type of foot contact.

Another class of constraints that are important are *unilateral constraints*, h_c for $c \in \mathcal{C}$, which are scalar valued functions, $h_c : Q \to \mathbb{R}$, that dictate the set of admissible configurations of the system; that is $h_c(q(t)) \geq 0$ implies that the configuration of the system is admissible for the contact point c. In the case of

foot contact, assuming that the walking is on flat ground, these constraints are the height of a contact point above the ground: $h_c(q(t)) = p_c^y(q(t)) \geq 0$. These can be put in the form of a matrix $h(q(t)) \in \mathbb{R}^{|Q|\times|Q|}$ in the same manner as holonomic constraints.

Domain Breakdowns. A domain breakdown is a directed cycle together with a specific choice of contact points on every vertex of that graph. To define this formally, we assign to each vertex a binary vector describing which contact points are active in that domain.

Definition 2. *Let $\ell = (V, E)$ be a cycle and $\mathcal{C} = \{c_1, c_2, \ldots, c_k\}$ a set of contact points. A domain breakdown is a function $\mathcal{B} : \ell \to \mathbb{Z}_2^k$ such that $B(v)_i = 1$ if c_i is in contact on v and $B(v)_i = 0$ otherwise.*

Example 2. *In the case of the graph Γ_u given in Example 1 and set of contact points $\mathcal{C} = \{lh, lt, rh, rt\}$, for the domain breakdown given in Fig. 1, this domain breakdown is formally given by $\mathcal{B}_u : \ell_u \to \mathbb{Z}_2^4$ where $\mathcal{B}_u([lh, lt])$, $\mathcal{B}_u([lt])$, $\mathcal{B}_u([lt, rh])$ and $\mathcal{B}_u([lt, rh, rt])$ are given by:*

$$\mathcal{B}_u(\ell): \begin{bmatrix} 1 \\ 1 \\ 0 \\ 0 \end{bmatrix} \to \begin{bmatrix} 0 \\ 1 \\ 0 \\ 0 \end{bmatrix} \to \begin{bmatrix} 0 \\ 1 \\ 1 \\ 0 \end{bmatrix} \to \begin{bmatrix} 0 \\ 1 \\ 1 \\ 1 \end{bmatrix}.$$

Note that in this case the choice of "left" and "right" leg is arbitrary, as long as it is kept consistent throughout the definition. The terms stance and non-stance leg are often used in the literature as well, but with the existence of double support phases this choice also becomes arbitrary.

2.3. Hybrid System Construction

We can now demonstrate that given a Lagrangian, a directed cycle, and a domain breakdown a hybrid system can be explicitly constructed. Since the Lagrangian is intrinsic to the robot being considered, this implies that a domain breakdown alone dictates the mathematical model of the biped.

Continuous Dynamics. The domain of the hybrid system is the direct product of the tangent space of the configuration space of the robot and the input space U which is dictated by the set of available actuators on the robot. The vector field in each mode is constructed by imposing the constraints as specified by the domain breakdown. For the mode $v \in V$, the holonomic constraints that are imposed are given by:

$$\eta_v(q(t)) = \eta(q(t))\mathcal{B}(v), \tag{4}$$

where the domain breakdown dictates which constraints are enforced. Differentiating the holonomic constraint yields a *kinematic constraint*:

$$J_v(q(t))\dot{q}(t) = 0, \tag{5}$$

where $J_v(q(t)) = \text{RowBasis}\left(\frac{\partial \eta_v(q(t))}{\partial q}\right)$ is a basis for the row space of the Jacobian (this removes any redundant constraints so that J_v has full row rank). The kinematic constraint yields the *constrained dynamics* in that mode:

$$D(q(t))\ddot{q}(t) + H(q(t), \dot{q}(t)) = B(q(t))u(t) + J_v(q(t))F_v(q(t), \dot{q}(t), u(t)) \quad (6)$$

which enforces the holonomic constraint; here D, H and B are as in Equation (3) and $F_v(q(t), \dot{q}(t), u(t))$ is a *wrench* [20]. To determine the wrench $F_v(q(t), \dot{q}(t), u(t))$, we differentiate the kinematic constraint and combine this result with Equation (6):

$$F_v(q, \dot{q}, u) = J_v^{-1}(q)\left[D(q)J_v^{-1}(q)\left(\dot{J}_v(q)\dot{q}\right) + H(q, \dot{q}) - B(q)u\right], \quad (7)$$

where we have suppressed the dependence on t in $q, \dot{q}$, and u. Therefore, for $x(t) = (q(t), \dot{q}(t))$, substituting Equation (7) into Equation (6) yields the control vector field $f_v(x(t), u(t))$. Importantly, notice that only the holonomic constraints but not the unilateral constraints appear in the control vector field and that the actual position to be maintained by the contact point as dictated by the holonomic constraints never appears inside of the control vector field.

Discrete Dynamics. We now construct the guards and reset maps for a hybrid system using the domain breakdown. From the wrench $F_v(q(t), \dot{q}(t), u(t))$, one can ensure that the contact point is enforced by considering inequalities on the friction which can be stated in the form: $\mu_v(q(t))^T F_v(q(t), \dot{q}(t), u(t)) \leq 0$, with $\mu_v(q(t))$ a matrix of friction parameters and constants defining the geometry of the contact point (see [19] for more details). These are coupled with the unilateral constraint in each mode, $h_v(q(t)) = h(q(t))\mathcal{B}(v)$, to yield the set of admissible configurations:

$$A_v(q(t), \dot{q}(t), u(t)) = \begin{bmatrix} \mu_v(q(t))^T F_v(q(t), \dot{q}(t), u(t)) \\ h_v(q(t)) \end{bmatrix} \leq 0. \quad (8)$$

The guard is just the boundary of the domain with the additional assumption that the set of admissible configurations is decreasing, i.e., the vector field is pointed outside of the domain, or for an edge $e = (v, v') \in E$,

$$G_e = \{(q, \dot{q}, u) \in TQ \times U : A_v(q, \dot{q}, u) = 0 \text{ and } \dot{A}_v(q, \dot{q}, u) \leq 0\}, \quad (9)$$

where we have suppressed the dependence on t in $q, \dot{q}$, and u. The reset map is derived by considering the impact equations which are given by considering the constraints enforced on the subsequent mode. For an edge $e = (v, v') \in E$, the post-impact velocity $\dot{q}(t^+)$ is given in terms of the pre-impact velocity $\dot{q}(t^-)$ and determines the reset map:

$$R_e(q(t^-), \dot{q}(t^-)) = \begin{bmatrix} q(t^-) \\ (I - D^{-1}J_{v'}^T(J_{v'}D^{-1}J_{v'}^T)^{-1}J_{v'})\dot{q}(t^-) \end{bmatrix}, \quad (10)$$

where I is the identity matrix, $J_{v'}$ is the Jacobian matrix in mode v', D is the inertia matrix, and we have suppressed the dependence on $q(t)$ in the Jacobian and inertial matrices. The result of this analysis is that given a domain

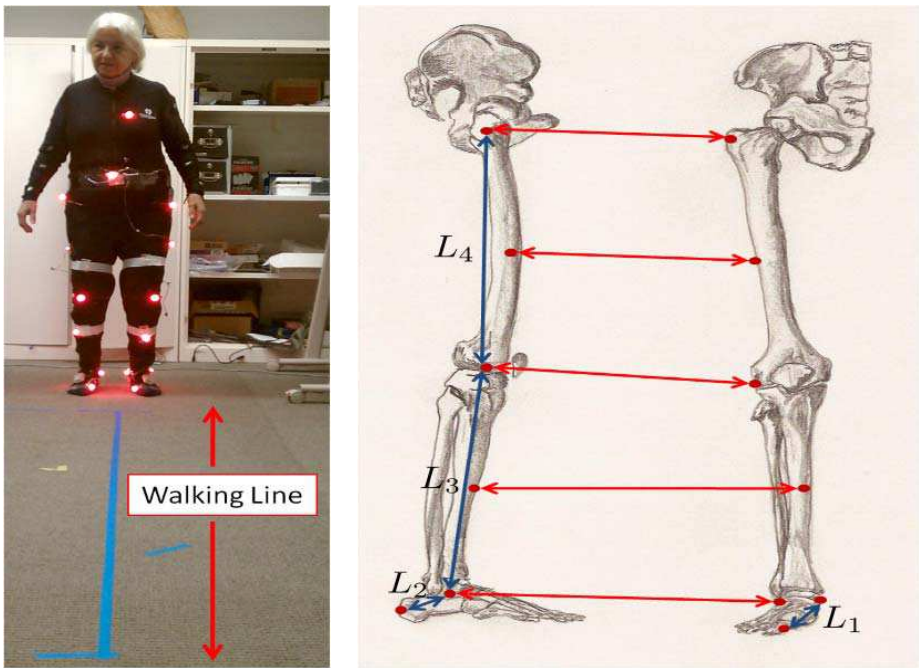

Figure 3: Illustrations of the experimental setup (left) and sensor placement on each foot (middle and right). Each subject in the experiment was required to wear a suit where the sensors (colored in red LEDs) are fastened in place. Each sensor was placed at the joints as illustrated with the red dots on the right lateral (middle) and anterior aspects (right) of the right leg. Sensors are placed identically on the left leg. The same sensors drawn from different views are connected with red arrows (right) and the labeled blue arrows are used to illustrate the diversity of subjects in Table 4.

breakdown and a bipedal robot (which determines just the unconstrained Lagrangian), the hybrid model for the biped is completely determined. If we then segment the empirically observed human walking by considering the sequence of contact point enforcements, we can extract a hybrid model for a biped that is capable of generating human-like gait.

3. Experimental Setup

In this section, we describe the experimental setup employed during data collection and describe the preprocessing done before determining the domain breakdown for each individual. After reading the description presented in this section, any interested researcher should be able to perform analysis on the

	Sex	Age	Weight	Height	L_1	L_2	L_3	L_4
1	M	30	90.7	184	14.5	8.50	43.0	44.0
2	F	19	53.5	164	15.0	8.00	41.0	44.0
3	M	17	83.9	189	16.5	8.00	45.5	55.5
4	M	22	90.7	170	14.5	9.00	43.0	39.0
5	M	30	68.9	170	15.0	8.00	43.0	43.0
6	M	29	59.8	161	14.0	8.50	37.0	40.0
7	M	26	58.9	164	14.0	9.00	39.0	41.0
8	F	77	63.5	163	14.0	8.00	40.0	42.0
9	F	23	47.6	165	15.0	8.00	45.0	43.0

Figure 4: Table describing each of the subjects. The measurements in column 4 are in kilograms and the measurements in column 5 are in centimeters.

collected data[1].

The data presented in this paper is collected using the Phase Space System[2], which computes the 3D position of 19 LED sensors at 480 frames per second using 12 cameras at 1 millimeter level of accuracy. The cameras were calibrated prior to the experiment and were placed to achieve a 1 millimeter level of accuracy for a space of size 4 by 4 by 4 meters cubed. 8 LED sensors were placed on each leg as Fig. 3 illustrates. 1 LED sensor was placed on the sternum, 1 LED sensor was placed on the back behind the sternum, and 1 LED sensor was placed on the belly button. Each sensor was fastened to subjects in a manner that ensured that they did not move during the experiment.

Each trial of the experiment required the subject to walk 3 meters along a line drawn on the floor (in Fig. 3 this line is drawn in blue). To simplify the data analysis each subject was required to place their right foot at the starting point of the line at the outset of the experiment and was told to walk in a natural manner. Each subject performed 12 trials, which constituted a single experiment. 3 female and 6 male subjects with ages ranging between 17 and 77, heights ranging between 161 and 189 centimeters, and weights ranging between 47.6 and 90.7 kilograms. Table 4 describes the measurements of each of the subjects.

To make the data collected from walking experiment amenable to analysis, it was processed through a three-step procedure: interpolation, data rotation and averaging. Since the motion capture information drops out periodically due to self-occlusions, we first interpolate the data to compensate for sensors dropping out of contact with the camera. The result of this initial data processing is

[1]The collected data can be found at `http://www.eecs.berkeley.edu/~ramv/HybridWalker.html`

[2]`http://www.phasespace.com/hardware`

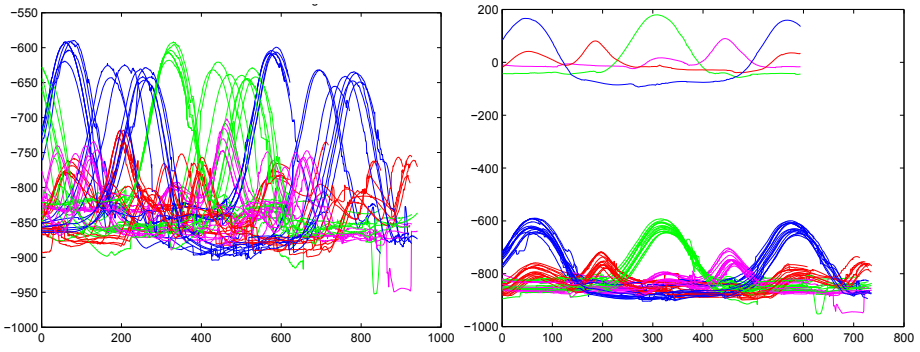

(a) Original Data (b) Postprocessed Data

Figure 5: (a) The data for the height (in mm) of the heel and toe for each leg for all 12 trials of a single individual and (b) the data after it has been shifted (drawn at the bottom of the plot) and averaged (drawn at the top of the plot after it has been shifted to have zero mean). Each color corresponds to a particular sensor.

relatively clean data over the course of a few steps (with the number of steps depending on the individual). From each of the trials, at least two steps are isolated (one with the right leg and another with the left leg) by ensuring that the data repeats. The data is then rotated so that the walking occurs in the x-direction. Since we are only interested in the data corresponding to constraint enforcement, only the sensor data for the heel and toe on each leg are considered (this is drawn in Fig.5(a)). For each subject, this data is considered for all 12 walking trials and averaged (after appropriately shifting the data in time) which results in a single trajectory for each constraint for each subject for at least two steps (one step per leg); this is the data that is used to determine the domain breakdown and is drawn in Fig.5(b).

4. Domain Breakdown

In this section, we present our approach to determining when and which constraints are enforced through the course of a step. More explicitly, the purpose of this section is to determine the specific time intervals during a step when the constraints are enforced. Doing so allows for a temporal ordering of events, yielding a domain breakdown. This would appear to be a simple task—for example, in the case of the heel, one need only determine when it is or is not on the ground—but this turns out to be non-trivial.

The obvious approach to determining the domain breakdown based upon the human data is to threshold the data, i.e., below the threshold a given constraint (heel or toe) is enforced and above it, it is not. Unfortunately due to the noisy nature of the data for the constraints "near the ground," choosing a proper threshold occurs at the scale of the noise. Smoothing the data aggressively can

"essentially" solve this problem, but then there becomes too many subject specific defined parameters in the domain fitting, i.e. the degree of smoothing and the threshold. This makes the resulting domain breakdown found through this process too user dictated. It is desirable to, instead, have a domain breakdown that is chosen "automatically," i.e., a domain breakdown that is independent of choices on thresholds and other parameters. To overcome this problem, we employ the notion of persistent homology and barcodes which were introduced in [21]. After describing this procedure, we illustrate how it can be employed to find a domain breakdown.

4.1. Persistent Homology

Before illustrating persistent homology, we begin by defining simplicial complexes and homology. The reader is encouraged to read [22] for a more complete introduction.

Definition 3. *A **simplicial complex** is a set K, together with a collection Ω of subsets of K called **simplices** such that for all $v \in K$, $\{v\} \in \Omega$, and if $\sigma \subseteq \omega \in \Omega$, then $\sigma \in \Omega$. We call the sets $\{v\}$ the **vertices** of K.*

Definition 4. *We say $\omega \in \Omega$ is a **k-simplex of dimension k** if $|\omega| = k + 1$ where $|\omega|$ denotes the cardinality of the set ω. An **orientation** of a k-simplex $\omega = \{v_0, \ldots, v_k\}$, is an equivalence class of orderings of the vertices of ω, where $\{v_0, \ldots, v_k\} \sim \{v_{\tau(0)}, \ldots, v_{\tau(k)}\}$. We denote an oriented simplex by (ω).*

Definition 5. *The **kth chain group** C_k of K is the free Abelian group on its set of oriented k-simplices, where if $(\omega) = -(\sigma)$ if $\omega = \sigma$ and σ and τ are differently oriented. An element $c \in C_k$ is a k-chain, $c = \sum_i n_i(\omega_i)$, $\omega \in K$ with coefficients $n_i \in \mathbb{Z}$.*

When it is clear from context what Ω is, we refer to the set K as a complex. For completeness, we set $C_{-1} = 0$. Though these simplicial definitions seem complicated, homology provides a means for a straightforward algebraic description of each simplicial complex.

Definition 6. *The **boundary operator** $\partial_k : C_k \to C_{k-1}$ is a homomorphism defined linearly on a chain $c \in C_k$ by its action on any simplex $\omega = (v_0, v_1, \ldots, v_k) \in c$, $\partial_k \omega = \sum_i (-1)^i (v_0, v_1, \ldots, \hat{v_i}, \ldots, v_k)$, where $\hat{v_i}$ indicates that v_i is deleted from the sequence. The boundary operator connects the chain groups into a **chain complex** C_*. We may also define subgroups of C_k using the boundary operator: the **cycle group** $Z_k = ker\, \partial_k$, and the **boundary group** $B_k = im\, \partial_{k+1}$ The k-**th homology group** is the quotient group $H_k := Z_k / B_k$. The* **homology** *of a complex is the collection of all homology groups. The rank of H_k is the k-**th Betti number** β_k.*

The Betti numbers of a chain group carry an important topological meaning. β_0 is equal to the number of connected components in a chain group and β_k for $k > 0$ is equal to the number of k-dimensional holes in a chain group. Though we

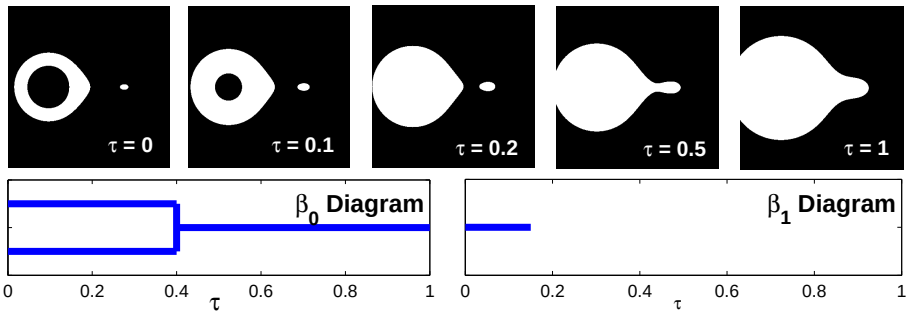

Figure 6: Snapshots for an image thresholded by $\tau \in [0, 1]$. The collection of thresholded images start with two connected components which merge at $\tau = 0.4$ as shown in the β_0 diagram. A hole is present until $\tau = 0.15$ as depicted in the β_1 diagram.

do not prove it here, continuous deformations of simplicial complexes preserve these Betti numbers. Therefore, the Betti numbers in a topological sense fully characterize a simplicial complex.

Given these definitions, we can now illustrate persistent homology. Suppose we construct a simplicial complex by thresholding an image over its intensity values and treating each pixel in the image as a node in the complex. Edges between nodes would arise when neighboring pixels in the thresholded image shared the same intensity value. An example of the application of this procedure to an image as a function of a threshold, τ, can be found in Fig. 6.

It is possible to track the Betti numbers as a function of the parameter τ. Most importantly, these features have a "life span" corresponding to the time at which the feature is introduced and the time at which disappears. For example, Fig. 6 shows the collection of complexes start with two connected components which eventually merge at $\tau = 0.4$. It also shows that the collection of complexes start with a hole that disappears at $\tau = 0.15$. This information is depicted as a persistence diagram at the bottom of Fig. 6. In particular, we notice that for any threshold greater than $\tau = 0.4$ corresponds to the most *persistent* topologically identical description of the image (i.e. the number of connected components and the number of holes are unchanged by choosing any larger threshold. As we describe in the next subsection, we employ the sensor data to construct a simplicial representation as a function of a threshold for the contact constraints that are enforced. After doing so we search for the threshold corresponding to the most persistent topological description of the data.

4.2. Determining the Domain Breakdown

In order to apply the persistent homology argument to determine a domain graph, we must describe how given a set of distinct thresholds for each motion capture sensor we construct a simplicial complex. Let the two toe and two heel sensors time series data, be denoted as $f_{lh}, f_{lt}, f_{rt}, f_{rh} : [0, T] \to \mathbb{R}$. Given a set of thresholds for each sensor, $\tau \equiv (\tau_{lh}, \tau_{lt}, \tau_{rh}, \tau_{rt})$, and encoding each combination

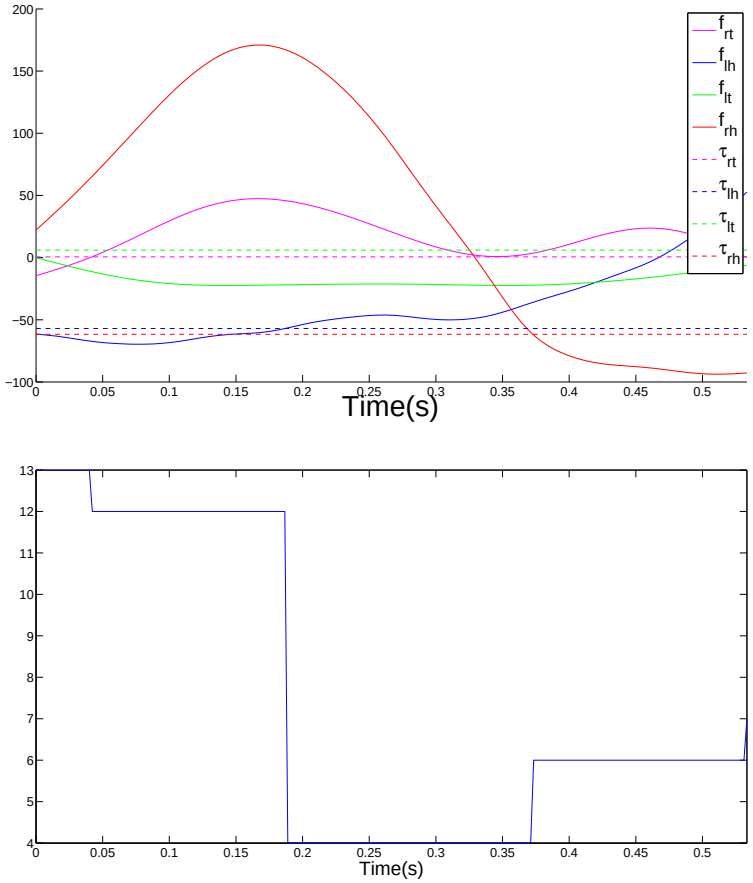

Figure 7: An illustration of the procedure to construct a simplicial complex from motion capture sensor data (top) via $C(\cdot, t)$ (bottom). For convenience we have transformed each combination of contact points, from $\mathbb{Z}_2^4$ to its decimal expansion.

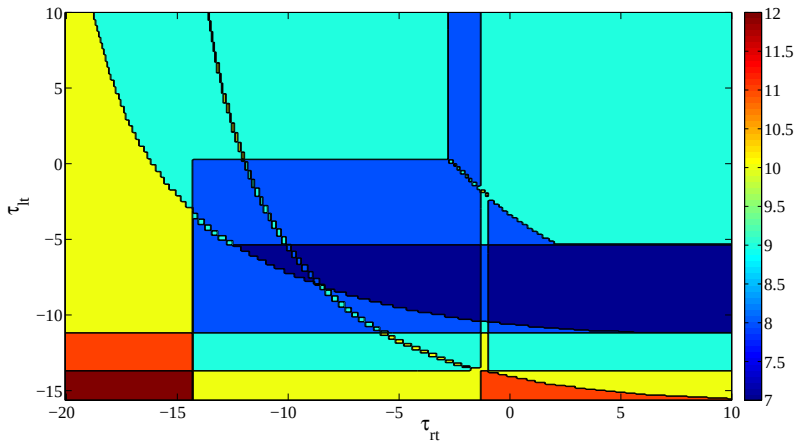

Figure 8: An illustration of β_0 as a function of τ_{rt}, τ_{lt}. Notice the the most persistent region corresponds to $\beta_0 = 9$.

of contact points as an element of $\mathbb{Z}_2^4$ (as we did in Example 2), we can define a function, $C : \mathbb{R}^4 \times [0, T] \to \mathbb{Z}_2^4$, which describes which set of constraints is active at a given time:

$$C(\tau, t; f_{lh}, f_{lt}, f_{rt}, f_{rh}) = \begin{bmatrix} \mathbb{1}\{f_{lh}(t) < \tau_{lh}\} \\ \mathbb{1}\{f_{lt}(t) < \tau_{lt}\} \\ \mathbb{1}\{f_{rh}(t) < \tau_{rh}\} \\ \mathbb{1}\{f_{rt}(t) < \tau_{rt}\} \end{bmatrix}. \tag{11}$$

Fig. 7 illustrates C for a given threshold. Given this function and a threshold, τ we can define a simplicial complex, K^τ. The $0-$simplices of K^τ correspond to all combinations of contact points (i.e. we would have 16 $0-$simplices). The $1-$simplices of K^τ correspond to transitions within the function C. That is, if $C(\cdot, t^-) = v_1$ and $C(\cdot, t^+) = v_2$ where $v_1 \neq v_2$, then we include the $1-$simplex $\{v_1, v_2\}$ in K^τ. For the illustration in Fig. 7 the $1-$ simplices in K^τ are $\{[lh, lt], [lt]\}$,$\{[lt], [lt, rh]\}$,$\{[lt, rh], [lt, rh, rt]\}$. Importantly each simplicial complex corresponds uniquely to a domain breakdown.

As we described earlier, we can compute the Betti numbers for each of these simplicial complex, K^τ. Fig. 8 illustrates how the number of connected components changes as a function of the thresholds for the toe sensors for a particular individual. Importantly, we notice that there is a large set of thresholds which result in a topologically similar domain graph. We employ the persistence homology argument to search over the space of thresholds to find the most topologically persistent domain breakdown (i.e. the threshold which corresponds to the most persistent number of connected components and cycles) and treat this as the domain graph corresponding to the walker.

In practice, naïvely searching over all possible thresholds (i.e. letting the

threshold be any value between $(-\infty, \infty)$) for the most persistent domain breakdown would result in the construction of a single domain, domain graph corresponding to either all the constraints being active or none being active. Therefore, some care must be taken in choosing an interval of interest over which to perform the thresholding. Since the subjects performed a walking experiment, at any instance at least one toe constraint was active and at least once each toe constraint was inactive which allows us to immediately restrict the space of thresholds for each toe over which to perform the analysis. Similarly each heel constraint was active and inactive at least once during the experiment allowing us to restrict the space of thresholds for each heel.

4.3. Results

After performing the aforementioned procedure, we consider the domain breakdowns for the various subjects. In particular, we notice as illustrated in Fig. 9 that in spite of the vast differences in age, height, and weight all subjects exhibit the *universal* domain breakdown which is shown in Fig. 1. This is particularly surprising, since we made no *a priori* assumptions about the ordering of constraint enforcement and did not demand simultaneous constraint enforcement between legs. Importantly, the similarities between the various walkers hints at the level at which to construct a cost function that when minimized produces human gait.

5. Cost of Walking from Human Data

While constructing a bipedal walking robot, beyond the immediate goal of obtaining stable walking, a cost function is generally chosen to optimize certain system parameters. The choice of cost function can have dramatic impacts on the resulting gait. In contrast to other robotic applications, the goal of bipedal walking is typically not to minimize some sort of energy expended, but rather to achieve the more nebulous goal of natural or human-like walking. The most popularly chosen cost functions applied to bipedal walking are torque squared [4, 19, 23] and the specific cost of transport [24, 25, 26]; however, no clear connection exists between minimizing these types of costs and achieving anthropomorphic walking. This lack of connection motivates the construction of a cost function based upon human walking data.

In this section, we construct a cost function that measures the anthropomorphic nature of robotic bipedal walking termed the *human-based cost*. We do this by first defining a metric on the space of weighted cycles, the *cut distance*, which allows us to compare different walking gaits and to construct an optimal walking cycle by minimizing the distance between the weighted cycles observed in the human walking data. Using the cut distance, we next define the *human-based cost* which allows us to compute the distance from a specific walking gait (either human or robotic) to the optimal walking cycle. The remainder of this section is devoted to using the human-based cost to determine the extent to which popular robotic models from the literature are anthropomorphic.

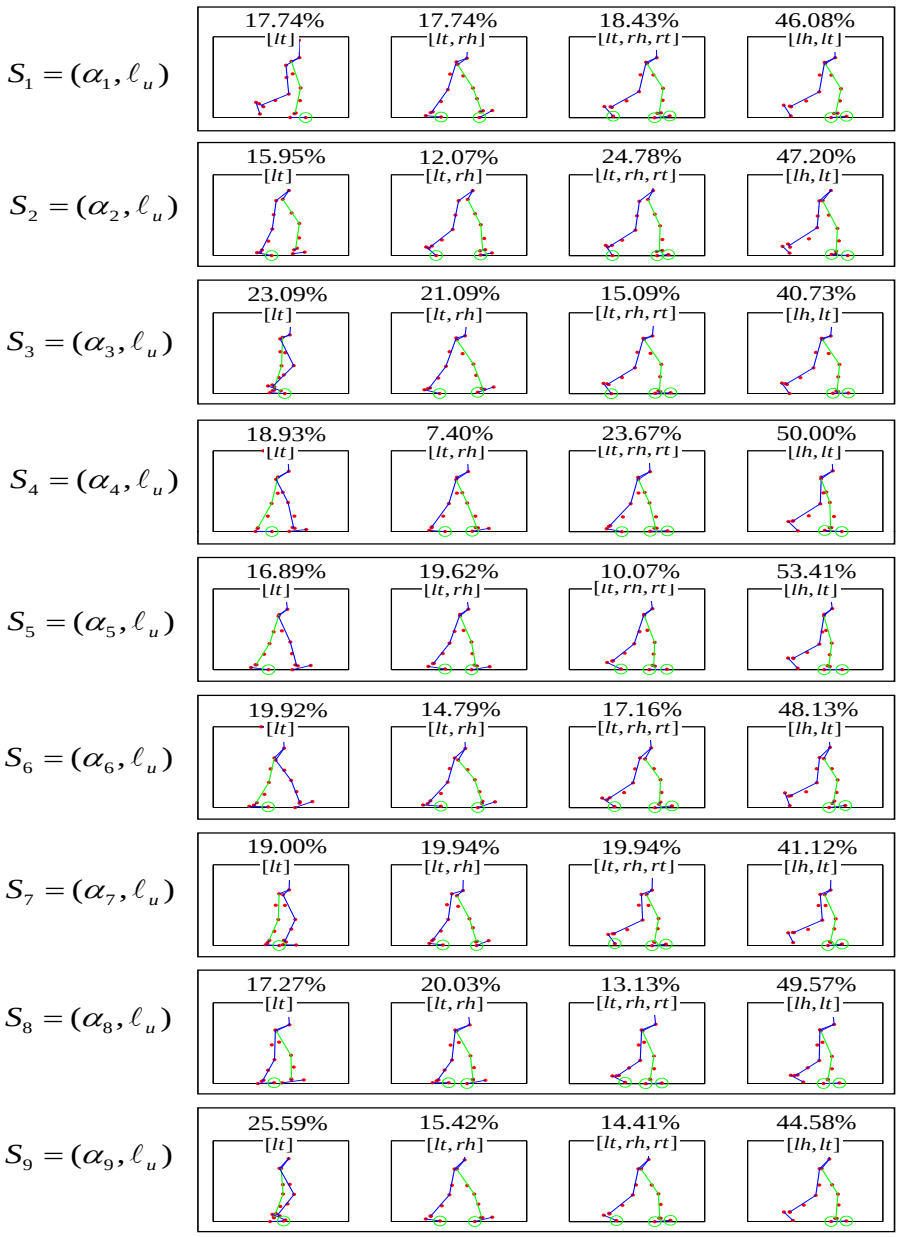

Figure 9: The domain breakdowns in each row for the 9 subjects in the order listed in 4 participating in the experiment. Comparing with the hybrid system illustrated in Fig. 1 the first through fourth rows correspond to $[lh, lt]$, $[lt]$, $[lt, rh]$, and $[lt, rh, rt]$, respectively. Each illustration is a snapshot of the subject's dynamics in the domain and above each plot is the percentage of the total gait spent within that domain.

5.1. Distance Between Cycles

We employ the notion of *cut* (or *rectangular*) distance between two weighted graphs to compare different domain breakdowns (the definition in its general form can be found in [27, 28]). Since we are only interested in the specific domains visited and the corresponding time spent in each of these domains, we define a notion of weighted cycle and a corresponding distance between weighted cycles that is pertinent to the application being considered.

Definition 7. *A walking cycle is a pair* (α, ℓ) *where* $\ell = (V, E)$ *is a cycle and* $\alpha : \ell \to \mathbb{R}^{|V|}$ *is a function such that* $\alpha(v) \geq 0$ *and* $\sum_{v \in V} \alpha(v) = 1$*. Denoting a cycle by* $\ell : v_0 \to v_1 \to \cdots \to v_p$*, we denote a walking cycle by:*

$$\alpha(\ell) : \alpha(v_0) \to \alpha(v_1) \to \cdots \to \alpha(v_p).$$

Example 3. *Each of the domain breakdowns presented in Fig. 9 gives us a distinct walking cycle. For example, Subject 1 has a walking cycle* $S_1 = (\alpha_1, \ell_1)$ *given by:*

$$\begin{array}{rcccccccc} \ell_1 & : & [lh, lt] & \to & [lt] & \to & [lt, rh] & \to & [lt, rh, rt] \\ \alpha_1(\ell_1) & : & 46.08\% & \to & 17.74\% & \to & 17.74\% & \to & 18.43\%. \end{array}$$

Here, and throughout this paper, weightings are stated in percentages to indicate the physical quantity that they represent: the time the human spends in a domain through the course of one step.

We now introduce a definition of cut distance that is a slight modification of the definition presented in [27, 28]. The only differences are that we do not force the weighted graphs to have nodes with positive weights, and we require the weights to sum to one.

Definition 8. *Let* $(\alpha_1, \ell_1 \equiv (V_1, E_1))$ *and* $(\alpha_2, \ell_2 \equiv (V_2, E_2))$ *be two walking cycles. Viewing both* α_1 *and* α_2 *as functions on* $V_1 \cup V_2$ *by letting* $\alpha_1(i) \equiv 0$ *if* $i \in V_2 \backslash V_1$ *and* $\alpha_2(j) \equiv 0$ *if* $j \in V_1 \backslash V_2$*, the cut distance between two cycles is given by:*

$$d(\alpha_1, \ell_1, \alpha_2, \ell_2) = \max_{I, J \subset V_1 \cup V_2} \left| \sum_{i \in I, j \in J} (\alpha_1(i)\alpha_1(j)\beta_1(i,j) - \alpha_2(i)\alpha_2(j)\beta_2(i,j)) \right| + \\ + \sum_{k \in V_1 \cup V_2} |\alpha_1(k) - \alpha_2(k)|, \tag{12}$$

where $\beta_1(i,j) = 1$ *for all edges* $(v_i, v_j) \in E_1$ *and* $\beta_2(i,j) = 1$ *for all edges* $(v_i, v_j) \in E_2$*.*

It is straightforward to check that the modified cut distance satisfies the requirements of a metric (i.e. non-negativity, identity of indiscernibles, symmetry and the triangle inequality). Intuitively, the cut distance compares just how different two walking cycles are when considering all possible "cuts" between the pair of cycles. To illustrate how the cut distance works, we consider a simple example:

Example 4. *Suppose we are given three walking cycles,* $W_i = (\alpha_i, \ell_i), i \in \{1, 2, 3, 4\}$*, defined as:*

$$\begin{array}{rcccc} \ell_1 & : & v_1 & & \\ \alpha_1(\ell_1) & : & 100\% & & \\ \ell_2 & : & v_2 & & \\ \alpha_2(\ell_2) & : & 100\% & & \\ \ell_3 & : & v_1 & \to & v_2 \\ \alpha_3(\ell_1) & : & 25\% & \to & 75\% \\ \ell_4 & : & v_1 & \to & v_2 \\ \alpha_4(\ell_2) & : & 50\% & \to & 50\%. \end{array}$$

We can then compute the cut distance between all pairs:

	W_1	W_2	W_3	W_4
W_1	0.000	3.000	2.500	2.000
W_2	3.000	0.000	1.500	2.000
W_3	2.500	1.500	0.000	0.625
W_4	2.000	2.000	0.625	0.000

where the entry in row j *and column* k *in the table corresponds to the cut distance between* W_j *and* W_k*.*

Notice that walking cycles that do not spend any time in the same domains are the furthest apart with respect to the cut distance. The transitions between pairs of vertices also play an important role during the comparison of the distance between pairs of walking cycles. For example, the net difference in node weights between W_3 and W_2 is the same as the net difference in node weights between W_3 and W_4. However, W_3 includes the same edges as W_4, but W_2 does not include the same edges as W_3; therefore, the distance between W_3 and W_2 is larger than the distance between W_3 and W_4.

5.2. Human-Based Cost

In this subsection, we develop a cost based upon the human domain breakdown and resulting walking cycles to judge non-human walking.

Definition 9. *Consider* N *subjects walking with associated domain breakdowns and a walking cycles* $S_i = (\alpha_i, \ell_i)$ $\forall\{1, \cdots, N\}$*. Letting* $\mathscr{L} = \bigcup_{i=1}^{N} \ell_i$ *be the graph obtained by combining all of the cycles* ℓ_i*. We define the optimal walking cycle by:*

$$(\alpha^*, \ell^*) = \underset{(\alpha,\ell)\in\mathbb{R}^{|\ell|}\times\mathscr{L}}{\operatorname{argmin}} \sum_{i=1}^{N} d(\alpha, \ell, \alpha_i, \ell_i). \tag{13}$$

The optimal walking cycle is just the walking cycle through the graph of all cycles obtained from the walking that best fits the data under the cut distance. The optimal walking cycle allows one to describe just how human-like a robotic walking gait is.

Definition 10. *Given a biped (either human or bipedal robot) with associated domain breakdown and walking cycle $R = (\alpha_r, \ell_r)$, the human-based cost (HBC) of walking is defined to be:*

$$\mathcal{H}(R) = d(\alpha_r, \ell_r, \alpha^*, \ell^*).$$

It is important to note that the optimal walking cycle may not be unique, and so there might be multiple HBC's of walking associated with a single experiment, i.e., the HBC is not necessarily unique (in this paper, we find a unique HBC). In addition, multiple experiments might yield different HBC's, but if they are carried out consistently they could be merged into a single HBC.

6. Computing the Human Based Cost

In this section, we consider the domain breakdowns for the 9 subjects in the walking experiment, $S_1 - S_9$. From these domain breakdowns, and the corresponding walking cycles, we compute the HBC. Since there is a unique cycle, it is unsurprising that there is a unique optimal walking cycle and therefore unique HBC. We show that the HBC gives useful information about the anthropomorphic nature of bipedal robotic models.

Using the walking cycles illustrated in Fig. 9, we now compute the optimal walking cycle and compute the HBC for the subjects and bipedal robots that have appeared in the literature. All the subjects have the same universal cycle ℓ_u and so $S_i = (\alpha_i, \ell_u)$ for $i = 1, \ldots, 9$ and the optimal walking cycle is given by (α^*, ℓ_u), where we compute α^* from (13) yielding:

$$\begin{array}{rcccccccc} \ell_u & : & [lh, lt] & \to & [lt] & \to & [lt, rh] & \to & [lt, rh, rt] \\ \alpha^*(\ell_u) & : & 46\% & \to & 19\% & \to & 18\% & \to & 17\%. \end{array}$$

We argue that if the objective is to obtain anthropomorphic bipedal walking, this optimal walking cycle should be matched as closely as possible. To demonstrate this, we use the optimal walking cycle to compute the HBC in several instances.

Humans. Although all of the subjects have the universal domain breakdown, this does not and should not imply identical walking gaits. To quantify the differences in walking between the different subjects, we compute the HBC for each subject. The results of this computation are illustrated in Fig. 10. Interestingly, nearly all of the human walkers exhibit nearly uniform HBC. This is unsurprising since the optimal walking cycle was constructed from their data, but the uniformity of their cost is particularly striking.

Robots. We next use the HBC to compute the cost of walking for bipedal robots that have been considered in the literature with no knee-lock. In [7] several bipedal models with a variety of domains (between 1 and 3) and walking gaits are considered. We focus on two of the domain graphs in [7]: $\ell_2 : [lh, lt] \to [lt]$ and $\ell_3^a : [lh, lt] \to [lt] \to [lt, rh, rt]$. Associated with the walking found in that paper, there are three walking cycles, $R_{2a} = (\alpha_{2a}, \ell_2)$, $R_{2b} = (\alpha_{2b}, \ell_2)$ and

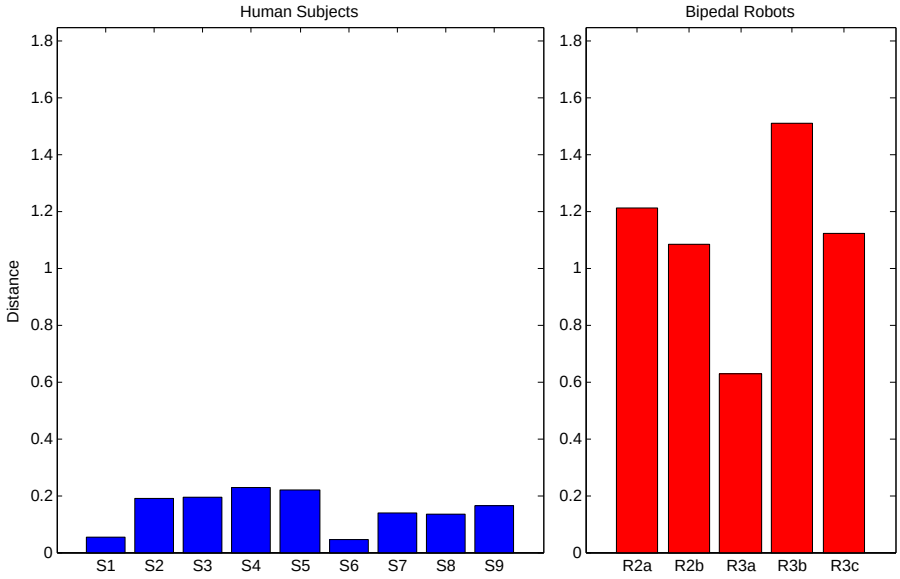

Figure 10: The HBC for the 9 subjects in the experiment, 5 bipedal robotic models that have appeared in the literature (with the number of domains in each of the models is illustrated by subscripts).

$R_{3a} = (\alpha_{3a}, \ell_3^a)$, given by:

$$\begin{array}{rcccc} \ell_2 & : & [lh, lt] & \to & [lt] \\ \alpha_{2a}(\ell_2) & : & 40\% & \to & 60\% \end{array}$$

$$\begin{array}{rcccc} \ell_2 & : & [lh, lt] & \to & [lt] \\ \alpha_{2b}(\ell_2) & : & 55\% & \to & 46\% \end{array}$$

$$\begin{array}{rccccc} \ell_3^a & : & [lh, lt] & \to & [lt] & \to & [lt, rh, rt] \\ \alpha_{3a}(\ell_3^a) & : & 44\% & \to & 43\% & \to & 13\%. \end{array}$$

Fig. 11 illustrates these robotic models.We compute the HBC for each of these models using α^* as illustrated in Fig. 10. From the results of the computed HBC, we conclude that the model R_{3a} produces the most anthropomorphic walking as it has a dramatically lower cost than the other two models. Interestingly enough, in that paper the authors state that this walking cycle "is the closest to human gait" amongst the ones they consider, which the HBC agrees with.

In [6] two bipedal walking gaits are obtained with a model consisting of a cycle: $\ell_3^b : [lh, lt] \to [lt] \to [rh]$, where $[rh]$ is a domain not seen in the human walking wherein the biped only has one contact point at the right heel (see Fig. 11 for an illustration). The paper considers two walking cycles $R_{3b} = (\alpha_{3b}, \ell_3^b)$

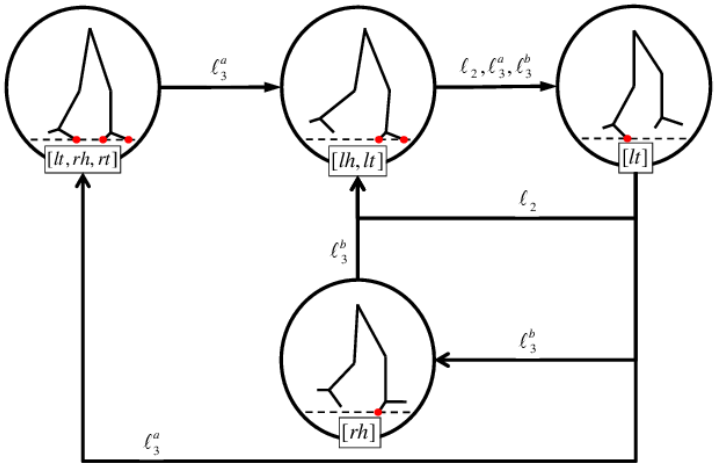

Figure 11: The domain breakdowns for the 5 robotic models without knee-lock considered in the literature.

and $R_{3c} = (\alpha_{3c}, \ell_3^b)$ given by:

$$\begin{array}{rcccccc} \ell_3^b & : & [lh, lt] & \to & [lt] & \to & [rh] \\ \alpha_{3b}(\ell_3^b) & : & 21\% & \to & 15\% & \to & 64\% \\ \ell_3^b & : & [lh, lt] & \to & [lt] & \to & [rh] \\ \alpha_{3c}(\ell_3^b) & : & 37\% & \to & 35\% & \to & 28\%. \end{array}$$

We compute the HBC for each of these models using α^* as illustrated in Fig. 10. Despite the fact that both of these models have three domains, they do not produce a lower HBC, which illustrates the fact that adding more domains does not necessarily result in more human-like walking. In particular, the high cost associated with these walking cycles is due to the $[rh]$ domain, which does not appear in human walking. Adding this domain was a design decision made by the authors; if, instead, the universal domain breakdown found from the human data were coupled with the techniques utilized in [6], it is very likely that a more anthropomorphic gait would have been constructed.

7. Conclusion

In this paper, we resolve an outstanding debate within the bipedal walking community by showing that there exists a *universal* temporal ordering of events during bipedal walking. We illustrate the existence of this *universal* temporal ordering by working from a motion capture dataset of a variety of subjects performing a straight line walking task and employing a novel automatized persistent homology technique to determine when constraints are active. The importance of our discovery is that it gives a single domain breakdown, and hence mathematical model, which can be used by all bipedal robot researchers. If consistency in the mathematical models can be achieved, any new controller developed that yields bipedal walking can be directly compared. Moreover, since this model is obtained directly from human walking, controllers developed using this domain breakdown promise to be more anthropomorphic.

The domain breakdowns and walking cycles which encode the amount of time spent in each discrete domain constructed from human data allow us to formulate a human-based cost which measures how anthropomorphic gait is. It was demonstrated that when the HBC was computed for the human subjects, preexisting medical conditions were successfully identified. When the HBC was computed for existing bipedal walking robots, the robots with more "human-like" walking gaits were correctly identified. This points to the utility of the HBC both in identifying medical conditions in humans, and in obtaining anthropomorphic walking in bipedal robots. The results of this paper also are applicable to future bipedal robot design. If the universal domain breakdown is used for the robotic model, and the parameters of the controller used to achieve walking are chosen so as to minimize the HBC, we postulate that the constructed gait will be more human-like.

References

[1] A. D. Ames, R. D. Gregg, M. W. Spong, A geometric approach to three-dimensional hipped bipedal robotic walking, in: 45th Conference on Decision and Control, San Diago, CA, 2007.

[2] A. Goswami, B. Thuilot, B. Espiau, Compass-like biped robot part I : Stability and bifurcation of passive gaits, rapport de recherche de l'INRIA (1996).

[3] R. Tedrake, T. Zhang, H. Seung, Learning to walk in 20 minutes, in: Proceedings of the Fourteenth Yale Workshop on Adaptive and Learning Systems, New Haven, Connecticut, USA, 2005.

[4] E. R. Westervelt, J. W. Grizzle, C. Chevallereau, J. Choi, B. Morris, Feedback Control of Dynamic Bipedal Robot Locomotion, Control and Automation, Boca Raton, FL, 2007.

[5] J. H. Choi, J. W. Grizzle, Planar bipedal walking with foot rotation, Portland, OR, 2005, pp. 4909–4916.

[6] T. Schaub, M. Scheint, M. Sobotka, W. Seiberl, M. Buss, Effects of compliant ankles on bipedal locomotion, in: IROS, St. Louis, Missouri, USA, 2009.

[7] D. Tlalolini, C. Chevallereau, Y. Aoustin, Comparison of different gaits with rotation of the feet for planar biped, Robotics and Autonomous Systems 57 (2009) 371–383.

[8] Y. Ogura, H. Aikawa, H. Lim, A. Takanishi, Development of a human-like walking robot having two 7-dof legs and a 2-dof waist, in: IEEE International Conference on Robotics and Automation, 2004., Vol. 1, IEEE, 2004, pp. 134–139.

[9] M. Popovic, A. Goswami, H. Herr, Ground reference points in legged locomotion: Definitions, biological trajectories and control implications, The International Journal of Robotics Research 24 (12) (2005) 1013–1032.

[10] T. Andriacchi, E. Alexander, Studies of human locomotion: past, present and future, Journal of Biomechanics 33 (10) (2000) 1217–1224.

[11] J. Rose, J. Gamble, I. Ovid Technologies, Human walking, Williams & Wilkins Baltimore, 1994.

[12] F. Zajac, R. Neptune, S. Kautz, Biomechanics and muscle coordination of human walking-Part I: Introduction to concepts, power transfer, dynamics and simulations, Gait and Posture 16 (3) (2002) 215–232.

[13] J. Perry, S. Thorofare, J. Davids, Gait analysis: normal and pathological function, Journal of Pediatric Orthopaedics 12 (6) (1992) 815.

[14] M. Whittle, Gait analysis: an introduction, Vol. 1, Butterworth-Heinemann Medical, 2002.

[15] D. A. Winter, Biomechanics and Motor Control of Human Movement, Hoboken, NJ, 2005.

[16] V. Zatsiorky, S. Werner, M. Kaimin, Basic kinematics of walking: step length and step frequency: a review, Journal of sports medicine and physical fitness 34 (2) (1994) 109–134.

[17] A. Ames, S. Sastry, A homology theory for hybrid systems: Hybrid homology, Hybrid Systems: Computation and Control (2005) 86–102.

[18] A. Ames, S. Sastry, Characterization of zeno behavior in hybrid systems using homological methods, in: American Control Conference, 2005. Proceedings of the 2005, IEEE, 2005, pp. 1160–1165.

[19] J. W. Grizzle, C. Chevallereau, A. D. Ames, R. W. Sinnet, 3d bipedal robotic walking: Models, feedback control, and open problems, in: NOLCOS, Bologna, Italy, 2010.

[20] R. M. Murray, Z. Li, S. S. Sastry, A Mathematical Introduction to Robotic Manipulation, Boca Raton, FL, 1993.

[21] G. Carlsson, A. Zomorodian, A. Collins, L. Guibas, Persistence barcodes for shapes, in: Proceedings of the 2004 Eurographics/ACM SIGGRAPH symposium on Geometry processing, ACM New York, NY, USA, 2004, pp. 124–135.

[22] A. Hatcher, Algebraic Topology, Cambridge University Press, 2002.

[23] C. Chevallereau, J. Grizzle, C. Shih, Asymptotically stable walking of a five-link underactuated 3D bipedal robot, IEEE Transactions on Robotics 25 (1) (2009) 37–50.

[24] M. Garcia, A. Chatterjee, A. Ruina, Speed, efficiency, and stability of small-slope 2D passive dynamic bipedal walking, in: Robotics and Automation, 1998. Proceedings. 1998 IEEE International Conference on, Vol. 3, IEEE, 2002, pp. 2351–2356.

[25] T. McGeer, Passive dynamic walking, The International Journal of Robotics Research 9 (2) (1990) 62.

[26] K. Ono, T. Furuichi, R. Takahashi, Self-excited walking of a biped mechanism with feet, The International Journal of Robotics Research 23 (1) (2004) 55.

[27] C. Borgs, J. Chayes, L. Lovász, V. Sós, K. Vesztergombi, Convergent sequences of dense graphs I: Subgraph frequencies, metric properties and testing, Advances in Mathematics 219 (6) (2008) 1801–1851.

[28] M. Deza, E. Deza, Encyclopedia of distances, Encyclopedia of Distances (2009) 1–583.